Caught in the Act: The Structure of Phosphorylated β-Phosphoglucomutase from *Lactococcus lactis*[†,‡]

Sushmita D. Lahiri,[§] Guofeng Zhang,[||] Debra Dunaway-Mariano,*[,||] and Karen N. Allen*[,§]

Department of Physiology and Biophysics, Boston University School of Medicine, Boston, Massachusetts 02118-2394, and Department of Chemistry, University of New Mexico, Albuquerque, New Mexico 87131

Received March 26, 2002; Revised Manuscript Received April 25, 2002

ABSTRACT: Phosphoglucomutases catalyze the interconversion of D-glucose 1-phosphate and D-glucose 6-phosphate, a reaction central to energy metabolism in all cells and to the synthesis of cell wall polysaccharides in bacterial cells. Two classes of phosphoglucomutases (α-PGM and β-PGM) are distinguished on the basis of their specificity for α- and β-glucose-1-phosphate. β-PGM is a member of the haloacid dehalogenase (HAD) superfamily, which includes the sarcoplasmic Ca^{2+}-ATPase, phosphomannomutase, and phosphoserine phosphatase. β-PGM is unusual among family members in that the common phosphoenzyme intermediate exists as a stable ground-state complex in this enzyme. Herein we report, for the first time, the three-dimensional structure of a β-PGM and the first view of the true phosphoenzyme intermediate in the HAD superfamily. The crystal structure of the Mg(II) complex of phosphorylated β-phosphoglucomutase (β-PGM) from *Lactococcus lactis* has been determined to 2.3 Å resolution by multiwavelength anomalous diffraction (MAD) phasing on selenomethionine, and refined to an $R_{cryst} = 0.24$ and $R_{free} = 0.28$. The active site of β-PGM is located between the core and the cap domain and is freely solvent accessible. The residues within a 6 Å radius of the phosphorylated Asp8 include Asp10, Thr16, Ser114, Lys145, Glu169, and Asp170. The cofactor Mg^{2+} is liganded with octahedral coordination geometry by the carboxylate side chains of Asp8, Glu169, Asp170, and the backbone carbonyl oxygen of Asp10 along with one oxygen from the Asp8-phosphoryl group and one water ligand. The phosphate group of the phosphoaspartyl residue, Asp8, interacts with the side chains of Ser114 and Lys145. The absence of a base residue near the aspartyl phosphate group accounts for the persistence of the phosphorylated enzyme under physiological conditions. Substrate docking shows that glucose-6-P can bind to the active site of phosphorylated β-PGM in such a way as to position the C(1)OH near the phosphoryl group of the phosphorylated Asp8 and the C(6) phosphoryl group near the carboxylate group of Asp10. This result suggests a novel two-base mechanism for phosphoryl group transfer in a phosphorylated sugar.

In this paper, we report the three-dimensional structure of the β-phosphoglucomutase from *Lactococcus lactis*. Both α- and β-phosphoglucomutases catalyze the interconversion of D-glucose-1-phosphate (G1P) and glucose-6-phosphate (G6P). This reaction is central to energy metabolism in all cells and is essential to the synthesis of cell wall polysaccharides in bacterial cells (*1*, *2*). The α-phosphoglucomutase (α-PGM) acts on the α-C(1) anomer of G1P, while the β-phosphoglucomutase (β-PGM) catalyzes the reaction of the β-C(1) anomer. Both mutases employ Mg^{2+} and β- or α-glucose 1,6-diphosphate (G1,6-diP) as cofactors (*1*, *2*). In addition, both mutases are monomeric proteins. The α-PGM (65 kDa) is, however, approximately twice the size of the β-PGM (25 kDa) (*3*). The X-ray structure of α-PGM from rat reveals a 4-domain α-/β-protein. All four domains contribute residues to form a large active-site crevice. The X-ray structure of β-PGM, reported here, is of a 2-domain α-/β-protein, which shares a common fold with the members of the haloacid dehalogenase (HAD) superfamily (*4*−*6*). The α-PGM and β-PGM do not have a common backbone fold, and, therefore, they must have evolved from different progenitors.

α-PGM and β-PGM catalysis proceeds via a phosphoenzyme formed by reaction of an active-site nucleophile with the cofactor glucose 1,6-diphosphate (*7*). Under physiological conditions, the mutase is maintained in its phosphorylated form. The α-PGM is phosphorylated at an active-site Ser residue (*8*) and the β-PGM at an active-site Asp (see below). The phosphorylated mutase binds either G1P or G6P and transfers the phosphoryl group to the C(6)OH or C(1)OH, respectively. Studies carried out on the rat α-PGM show that

[†] This work was supported by a grant from National Institute of Health GM16099 (to K.N.A. and D.D.-M.). Use of the Advanced Photon Source was supported by the U.S. Department of Energy, Basic Energy Sciences, Office of Science, under Contract No. W-31-109-Eng-38. Use of the BioCARS Sector 14 was supported by the National Institutes of Health, National Center for Research Resources, under Grant No. RR07707.

[‡] The coordinates of the refined structure have been deposited with the Protein Data Bank, accession code 1LVH.

* Correspondence should be addressed to Karen N. Allen, Department of Physiology and Biophysics, Boston University School of Medicine, 80 East Concord Street, Boston, MA 02118-2394, Tel: 617-638-4398, Fax: 617-638-4285, E-mail: allen@med-xtal.bu.edu or Debra Dunaway-Mariano, Department of Chemistry, University of New Mexico, Albuquerque, NM 87131, Tel: 505-277-3383, Fax: 505-277-6202, E-mail: dd39@unm.edu.

[§] Boston University School of Medicine.

[||] University of New Mexico.

10.1021/bi0202373 CCC: $22.00
Published on Web 06/05/2002

Scheme 1

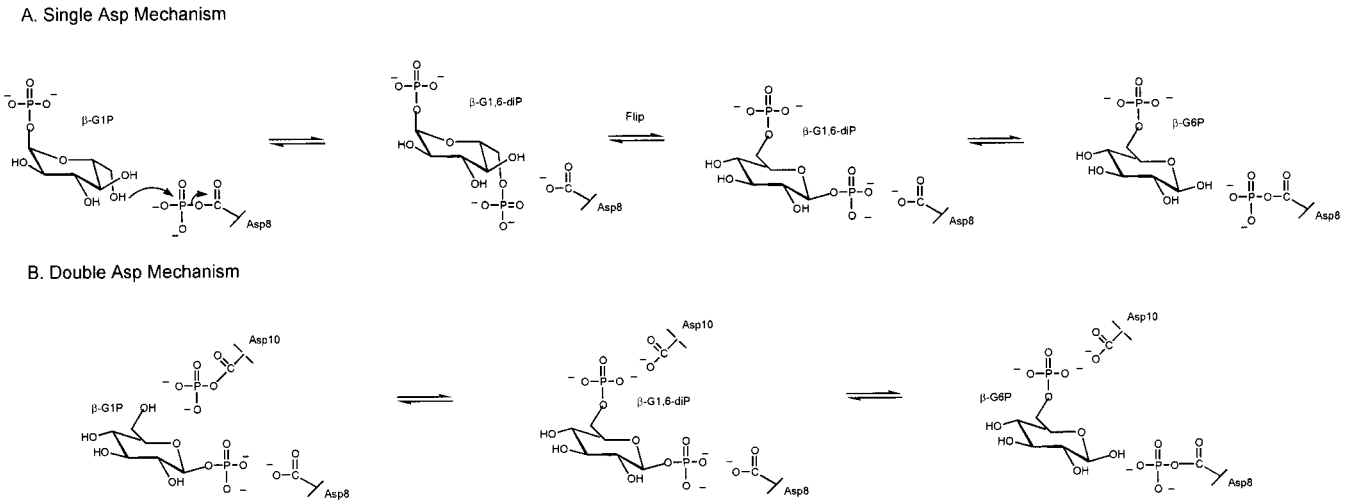

the glucose 1,6-diP formed reorients itself by "flipping" in the large active-site cleft rather than by dissociating and rebinding (*9*). The change in ligand orientation is necessary for the alignment of the phosphoryl group targeted for transfer with the single active-site nucleophile. The reaction cycle is completed upon phosphoryl transfer from the C(1)-phosphate or C(6) phosphate of the G1,6-diP to form phosphorylated enzyme and the corresponding product.

In view of the small active-site cavity observed in the X-ray structures of several of the β-PGM HAD family homologues [haloalkanoic dehalogenase (*4*), phosphonatase (*10*), and phosphoserine phosphatase (*11*)], it is difficult to imagine that the active site of β-PGM could accommodate the "flipping" of G1,6-diP observed for the α-PGM mechanism of catalysis. Thus, the G1,6-diP formed in the β-PGM active-site would have to dissociate into solvent and then bind again in the opposite orientation (Scheme 1A). An analysis of β-PGM active-site residues located on conserved active-site loops of the HAD family enzymes suggested to us that an alternative mechanism may be operative in the β-class of phosphoglucomutases. The β-PGM active site contains not only Asp8, which occupies the Asp nucleophile position found in each of the HAD family members, but also a neighboring aspartate, Asp10. As illustrated in Scheme 1B, both aspartate residues might function in phosphoryl transfer thus eliminating the need for reorientation of the G1,6-diP intermediate within the active site. Thus, by using a two-Asp mechanism, the phosphoryl transfer from position 1 to position 6 on the β-glucose might be accomplished within the confines of a small active-site crevice.

The first step taken in the elucidation of the mechanism of β-PGM catalysis was the determination of the X-ray crystal structure of the enzyme. The *Lactococcus lactis* β-PGM was isolated from an *Escherichia coli* clone in its phosphorylated form, and cocrystallized with Mg^{2+} (*12*). The structure, solved by X-ray crystallography at 2.3 Å resolution, provides the first "snapshot" of the β-PGM class of phosphoglucomutases, and a glimpse into the mechanism of catalysis. Moreover, from this structure we see for the first time in any HAD superfamily member the active site acyl-phosphate intermediate formed during the course of catalysis of phosphoryl transfer. The observed environment of the acyl-phosphate provides insight into how this intrinsically high-energy functional unit is preserved in the absence of substrate but activated for transfer in its presence.

EXPERIMENTAL PROCEDURES

Purification and Crystallization. Recombinant selenomethionine (SeMet) *Lactococcus lactis* β-PGM (*1*, *2*) was purified from the *E. coli* clone for crystallization as described in Lahiri et al. (*12*). Crystals of the native β-PGM were grown at pH 7.5 in the presence of 5 mM Mg^{2+} using the vapor-diffusion method with hanging drop geometry (*12*). Ammonium fluoride (0.1 M) and 16% w/v PEG 3350 were employed as the precipitating agents. The crystals belong to the spacegroup $P2_12_12_1$ with cell dimensions $a = 53.667$ Å, $b = 92.776$ Å, $c = 111.597$ Å and contain two molecules per asymmetric unit (*13*). Crystals were flash frozen in liquid nitrogen, using Paratone-N (Hampton Research) as cryoprotectant. Microseeding SeMet β-PGM with native β-PGM crystals during crystallization yielded SeMet β-PGM crystals that diffracted to 2.3 Å (*12*).

Data Collection and Processing. The three-wavelength multiwavelength anomalous diffraction (MAD) data set for SeMet β-PGM was collected to 2.3 Å on beamline BM 14C at Argonne National Laboratories using a CCD detector (*14*, *15*). MAD data were collected at three different wavelengths in 90° wedges with Bijvoet pairs collected using reverse-beam geometry for each wedge at 0.9792369 Å (edge), 0.9790073 Å (peak), and 0.96112713 Å (remote). The details of data collection are summarized in Table 1. The DENZO and SCALEPACK package (*16*) were used for determination of the unit-cell parameters, data indexing, reduction, and scaling.

MAD Phasing and Model Building. The structure was solved using MAD phasing of the SeMet derivative. Including the N-terminal methionine of each chain, three selenium atoms were expected in the SeMet derivative (replacing Met1, Met 83, and Met 126). SOLVE version 1.19 (*17*) was used to locate all three SeMet sites in each of the two molecules in the asymmetric unit. The map was improved slightly using solvent flattening in the program RESOLVE version 1.05 (*18*). Secondary structure elements and clear protein−solvent boundaries were easily discerned in the map. A polyalanine chain was fitted first into the density using

Table 1: Summarized Crystallographic and Refinement Statistics

unit cell dimensions (Å)	$a = 53.667$	$b = 92.776$	$c = 111.597$
space group	$P2_12_12_1$		
X-ray source	APS 14-BM-D		
data set	SeMet-λ_1 (edge)	SeMet-λ_2 (peak)	SeMet-λ_3 (remote)
wavelength (Å)	0.9792369	0.9790073	0.96112713
resolution range (Å)	50−2.3	50−2.3	50−2.3
total/unique reflections	420727/23862	419349/24329	421192/24089
completeness (%)[a]	91.0 (60.8)	95.7 (81.8)	92.9 (61.4)
I/σ (I)	12.3 (3.5)	18.0 (4.9)	17.6 (4.2)
R_{merge}[b] (%)	0.081 (0.17)	0.081 (0.19)	0.072 (0.19)
f'/f'' (e^-)	−10.7/3.5	−8.3/6.1	−9.9/2.9
figure of merit[c] to 3.0 Å (MAD/solvent flattened)	0.5/0.7		

Refinement Statistics	
no. of protein atoms/asymmetric unit	1712
no. of reflections (working/free set)	21745/2390
R_{work}[d]/R_{free}[e] (%)	0.24/0.28
average B factors (Å^2)	
amino acid residues	41.3
Mg^{2+} ions (2 total)	1.0
phosphate (2 total)	22.7
water (258 total)	39.8
r.m.s.	
bond length (Å)	0.007
angles (deg)	1.26

[a] Completeness of the outermost shell (2.38−2.3 Å) is shown in parentheses. [b] $R_{merge} = \sum_{hkl}\sum_i|I_{hkl,\,i} - \langle I_{hk}\rangle I|/\sum_{hkl}\sum_i|I_{hkl,\,i}|$, where $\langle I_{hkl}\rangle$ is the mean intensity of the multiple $I_{hkl,\,i}$ observations for symmetry related reflections. [c] Reported by SOLVE. [d] $R_{work} = \sum_{hkl}|F_{obs} - F_{calc}|/\sum_{hkl}|F_{obs}|$. [e] $R_{free} = \sum_{hkl\ \Sigma T}|F_{obs} - F_{calc}|/\sum_{hkl}|F_{obs}|$, where the test set T includes 10% of the data.

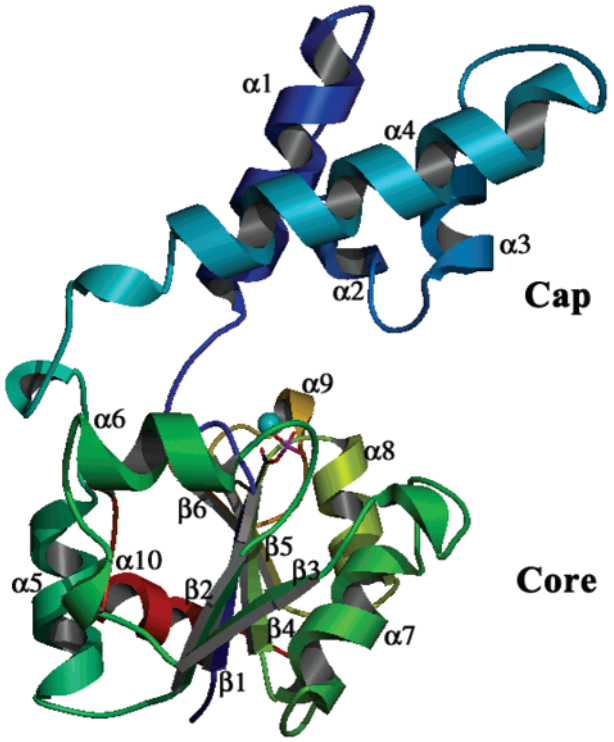

FIGURE 1: Structure of β-phosphoglucomutase. A schematic representation with the strands and helices labeled sequentially with color ramped from blue to red from N- to C-terminus. The aspartyl phosphate group (Asp8) is shown as a stick model and Mg^{2+} ion as a cyan sphere.

the molecular graphics package O (*19*). A total of 217 amino acid residues (out of 221 total) were built into one molecule. The selenium and aromatic residues were used to help register the amino acid sequence to the polyalanine chain. Once side-chains were fitted into the first monomer, the model was then translated to position the second monomer into density, using the selenium and aromatic residue positions as a guide. After the first three rounds of refinement (described below), the entire polypeptide model was complete with the exception of the four C-terminal amino acids that could not be fitted with confidence. At this point, the phosphate and the Mg^{2+} ions were placed into the strong electron density at the active site (as deduced from sequence alignment). There was no ambiguity in the placement of the liganded molecules in either subunit, because of the strong electron density of the Mg^{2+} ($>11\sigma$) and PO_4^{3-} ($>9\sigma$) in the sigmaa weighted $2F_o - F_c$ map (*20*).

Refinement. The initial round of refinement included rigid-body refinement and simulated annealing using torsional dynamics performed against a maximum likelihood/Hendrickson-Lattman (MLHL) minimization target incorporating the observed MAD phases from SOLVE using the program CNS-solve (*21*). For statistical cross-validation 10% of the data were excluded (for calculation of R_{free}). In the last stages of refinement, clear density at the C-termini allowed the chain to be extended by four additional amino acids, thus accounting for all the amino acids in the protein. The model was further refined using a combination of simulated annealing and minimization, alternating with manual rebuilding of the model using $2F_o - F_c$ and $F_o - F_c$ electron density maps. The final model was checked using a simulated annealing composite omit map. The automated water-picking program in CNS was used to assign water molecules in the structure, all of which were visible in the $F_o - F_c$ electron density map at 3σ. In the final stages, the group and individual B-factors were refined, resulting in final crystallographic R values of $R_{cryst} = 0.24$ and $R_{free} = 0.28$. Analysis of the Ramachandran plot showed 98% of 221 residues fall within the most favored region, 1.6% fall in the additionally allowed region, and only 0.4% fall in the generously allowed regions, as defined by PROCHECK (*22*). Model and refinement statistics are summarized in Table 1. Coordinates have been deposited in the Protein Data Bank (accession code 1LVH) for the SeMet protein.

RESULTS AND DISCUSSION

Overall Structure. Purified recombinant *Lactococcus lactis* β-PGM was crystallized in the presence of Mg^{2+} to yield its phosphorylated form. β-PGM is a monomer that is comprised of two distinct domains, a helical cap domain and an α/β core domain, with overall dimensions of 56 × 35 × 36 Å (see Figure 1). The core domain, which includes residues 1−14 and residues 93−221, is comprised of a centrally located six stranded parallel β-sheet ($\beta1-\beta6$) surrounded by six α-helices (α5−α10). Typical right-handed $\beta-\alpha-\beta$ connections are present. The cap domain, which includes residues 15−92, is inserted between $\beta1$ and α5 of the core domain. It consists of an antiparallel, four-helix bundle (α1−α4). Together the core and the cap domain give rise to a kidney-bean shaped monomer, similar to that seen in the structures of phosphonoacetaldehyde hydrolase (*10*) and phosphoserine phosphatase (*11*). Like these two phosphotransferases, β-PGM is a member of the haloacid dehaloge-

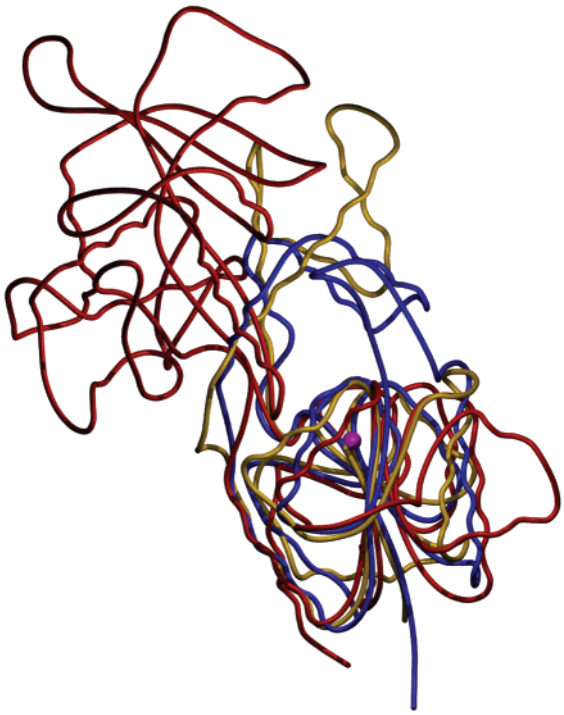

FIGURE 2: Overlay of the β-PGM Cα trace (gold) with that of phosphoserine phosphatase (blue), and the P-domain of Ca^{2+}-ATPase (red). The N-domain of Ca^{2+}-ATPase, which functionally corresponds to the cap domain of the other phosphotransferases, is also shown. The position of the phosphate of the aspartyl phosphate residue is shown as a purple sphere.

nase (HAD) enzyme superfamily as verified by the fact that it shares the common α/β core domain with other HAD family members. Figure 2 shows the superposition of the backbones of these three HAD family phosphotransferases. The average B-factor of the β-PGM cap domain is higher (*B* factor = 41.9) than that of the core domain (*B* factor = 26.58), consistent with the known mobility of the cap domain in several HAD structures (*4*, *10*, *11*).

Active-Site Structure. The active site of β-PGM is located at the domain−domain interface. The exact location is identified by the phosphorylated side chain of Asp8 and by the bound Mg^{2+} cofactor (Figure 1). The active site is comprised of the side chains of Lys45 and Thr16 contributed by the cap domain and the side chains of Asp8, Asp10, Val12, Ser114, Lys145, Glu169, and Asp170 contributed by the core domain (Figure 3). The 10 most closely related bacterial β-PGMs identified in a BLAST sequence alignment (*23*) conserve 29 out of the 221 amino acids of *Lactococcus lactis* β-PGM. Each of the active-site residues named is among these conserved residues. Moreoever, the Asp8 nucleophile, Asp10, Ser114, Lys145, Glu169, and Asp170 (β-PGM numbering) are conserved among all HAD phosphotranferases.

We observe two electron densities (in the $2F_o - F_c$ map) at high contour levels ($>9\sigma$) in the active site, one of which is the Mg^{2+} cofactor and the other, connecting to the nucleophilic Asp8 (<1.5 Å distance), is that of covalently bound phosphate (phosphoAsp 8) (Figure 3b). The presence of the connected density is in agreement with the biochemical data (*24*), which show that β-PGM exists as a stable phosphoenzyme. We note that no phosphate, sulfate, or similar ions were included in the crystallization solution, and thus the assignment of the electron density to a phosphoryl group covalently linked to Asp8 is unequivocal.

The Mg^{2+} is liganded with octahedral coordination geometry by the three carboxylate side chains of Asp8, Glu169, and Asp170, the backbone carbonyl oxygen of Asp10, one phosphoAsp8 phosphate oxygen, and a water molecule. The phosphate group of phosphoAsp8 is within hydrogen-bond distance of the hydroxyl group of Ser114 and the ammonium group of Lys145. Lys145 also forms a salt bridge with the carboxylate side chain of Asp8.

Mechanistic Implications. If β-PGM catalysis utilizes a single nucleophile (Scheme 1A) as does α-PGM, we can envision β-G1P binding to the β-PGM active site and undergoing phosphoryl transfer from the phosphoAsp8 to form β-G1,6-diP. Unlike the active site of α-PGM, the active site of β-PGM is not large enough for the bound β-G1,6-diP to "flip" into the correct orientation that would allow the ensuing in-line attack of the Asp8 carboxylate on the C(6) phosphoryl group to occur. Thus, we expect that once formed, the β-G1,6-diP would, by necessity, dissociate from the active site into solution and then return to the active site to bind in the correct orientation for transfer of the C(6) phosphoryl group to Asp8. However, on the basis of our analysis of the active-site template conserved among HAD family enzymes, we had anticipated that the structure of the β-PGM active site might be compatible with a two-nucleophile mechanism in which Asp8 and Asp10 function as the mediators of phosphoryl transfer (see Scheme 1B). To test the feasibility of this mechanism, we modeled β-G1P and β-G6P into the active site structure of phosphorylated β-PGM.

As shown in Figure 4, the active site with modeled β-G1P shows alignment of the C(6)OH with the phosphoryl group of the phosphoAsp8 and alignment of the G1P C(1) phosphoryl group with the Asp10 carboxylate. Lys145, Ser114, and Mg^{2+} are positioned to assist in the phosphoryl transfer reaction to Asp8 by balancing charge and orienting the reacting groups. The symmetry of the disposition of polar residues around the C(1) and C(6) sugar phosphate binding site is remarkable. If one draws a vertical line from the Mg^{2+} ion through the bridging oxygen of the sugar ring, the residues located on the left-hand side of the line: Ser114, Asp8, Lys145, Glu169 practically mirror those located on the right: Thr16, Asp10, Lys45, and Asp170. Thus, one can imagine one set of catalytic groups functioning in the phosphorylation of the sugar C(1)OH and the other set functioning in the phosphorylation of the sugar C(6)OH. In ongoing studies, kinetic and structural approaches are being used to distinguish between the classical (Scheme 1A) and the two-nucleophile (Scheme 1B) mechanisms of β-PGM catalysis. In this regard, it is interesting that the phosphoAsp8 form of β-PGM is isolated and not a mix of the phosphoAsp8 and phosphoAsp10 forms. This finding does not argue against a two-nucleophile mechanism since the phosphoAsp8 form may be more thermodynamically favorable or stabilizes the enzyme in a conformation favorable for crystallization.

Conservation of the HAD Fold and Specialization of the HAD Active-Site Scaffold. The structure of 2-L-haloalkanoic dehalogenase was the first of the HAD family to be defined (*4*, *25*). It is comprised of an α/β-core domain and a small α-/β-cap domain. Recently, we reported the X-ray structure of another family member, phosphonatase (*10*), which

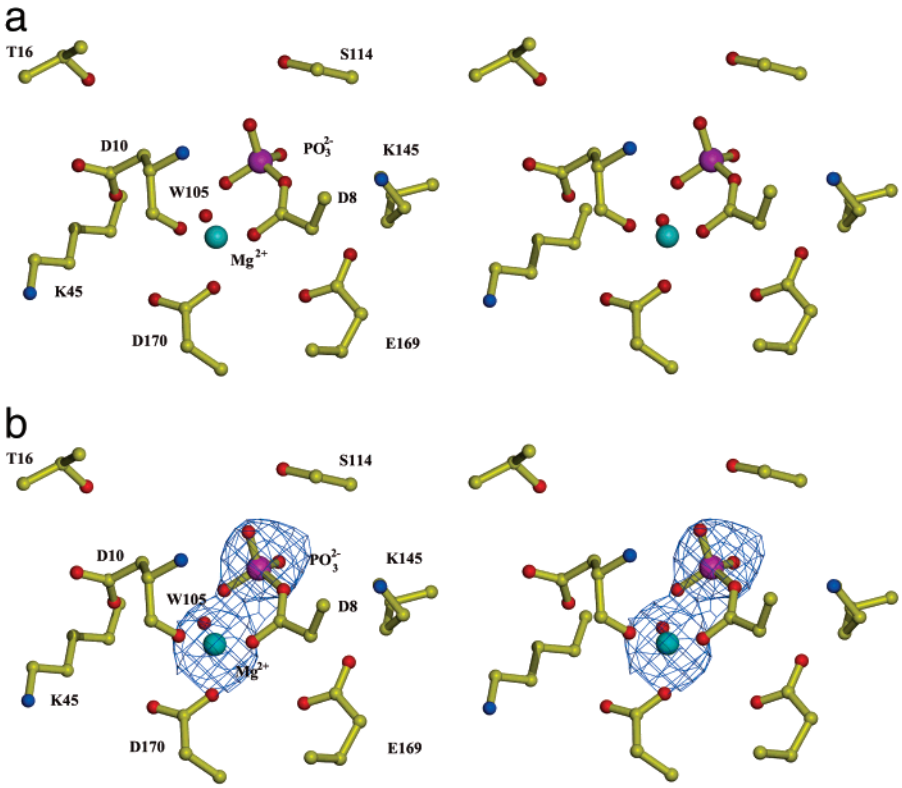

FIGURE 3: Active-site of β-PGM (a) stereoview of the protein residues in the active site along with the covalent phosphate (shown in magenta) and bound cofactor Mg^{2+} (shown in cyan). The water molecule liganded to the Mg^{2+} (W105) is also shown. (b) Stereoview of the active site residues with the $2F_o - F_c$ electron density map (contoured at a 3.5σ level) depicted as blue cages.

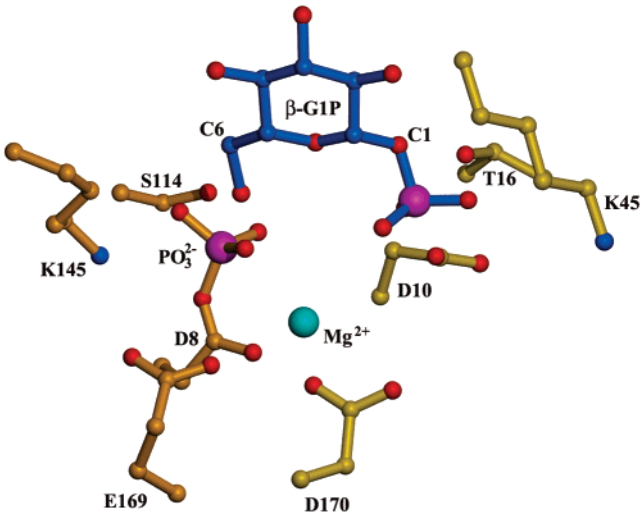

FIGURE 4: The active site of β-PGM showing the docked substrate glucose-1 phosphate and polar residues within 6 Å to the sugar C(1) and C(6). The residues located proximal to C(6) of the sugar are shown in gold and those located proximal to C(1) of the sugar are shown in yellow.

catalyzes the hydrolytic cleavage of the P−C bond in phosphonoacetaldehyde. Superposition of the two structures reveals a conserved active-site platform within the core domain comprised of four peptide loops (*10*) (see Figure 5 for superposition (a) and schematic (b)). These four loops correspond to the four conserved sequence motifs within the HAD enzyme family which had been noted previously by us (*10*, *26*) and by other investigators (*4*, *5*, *24*, *27*, *28*). The structures of 2-haloalkanoic acid dehalogenase (*4*), phosphonatase (*10*), Ca^{2+}-ATPase (*29*), phosphoserine phosphatase (*11*), and β-PGM show that loop 1 positions the conserved Asp nucleophile (and the acid/base catalyst in the phosphoserine phosphatase and Ca^{2+}-ATPase; see discussion below), loop 2 positions the substrate-binding Ser in the dehalogenase and the aspartyl phosphate binding Ser/Thr in the phosphotransferases, loop 3 positions the Lys, which orients the Asp nucleophile (and in the phosphotransferases also interacts with phosphoryl group of the aspartyl phosphate intermediate), while loop 4 positions the Asn/Asp pair, which functions in binding the water nucleophile in the dehalogenase, and the Asp/Asp pair, which functions in Mg^{2+} binding in the phosphotransferases.

We are most intrigued by how the four phosphotransferases have become specialized to perform their specific catalytic function. In brief, phosphonatase, phosphoserine phosphatase, and Ca^{2+}-ATPase deliver a phosphoryl group from the substrate to the active-site Asp and hence to water. The β-PGM, on the other hand, moves the phosphoryl group from one site on the substrate to another using an active-site Asp as mediator. For the three hydrolases, the requirements for acid−base catalysis are quite different. The phosphoserine phosphatase requires an acid group to protonate the serine alchoholate formed upon phosphoryl transfer to the active-site Asp. This role appears to be filled by Asp13. This residue is strategically positioned on segment 1, two residues removed from the Asp11 nucleophile. The Asp13 carboxylate anion thus formed can serve as a base catalyst in the hydrolysis of the phosphoaspartyl group. The position and protonation state of Asp13 would appear to be enforced through interaction with its close spatial neighbor Glu120. In contrast to the phosphoserine phosphatase, the ATPase does not require acid catalysis because the ADP leaving

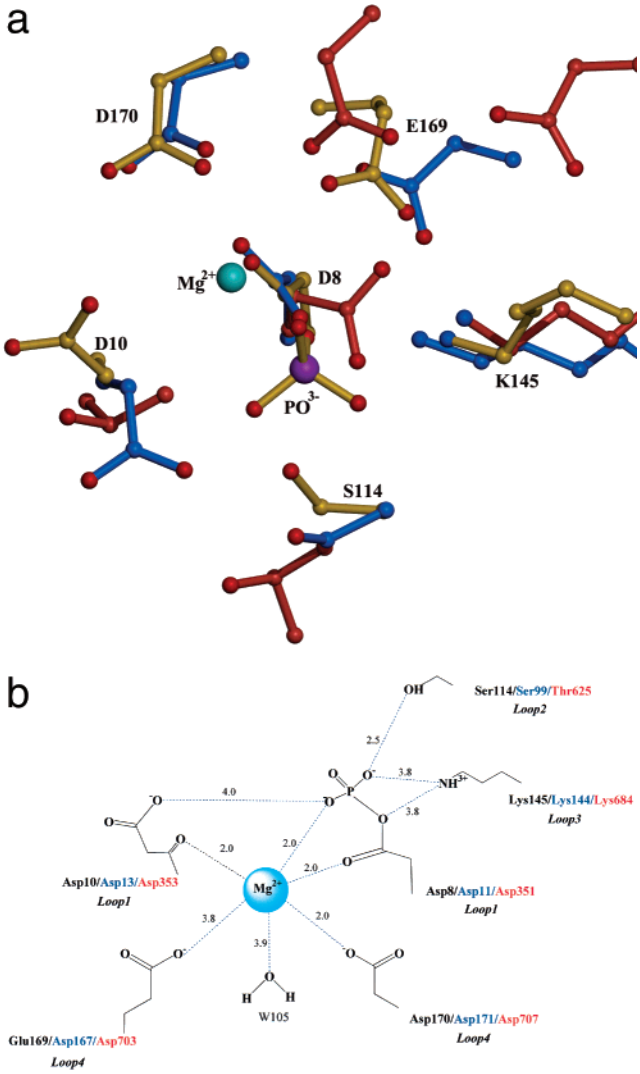

FIGURE 5: Comparison of the active-site residues of the three phosphotranferase members of the HAD superfamily, β-PGM (gold), phosphoserine phosphatase (blue), and P domain of Ca^{2+}-ATPase (red). (a) Superimposition of the active site residues (shown as ball-and-stick model) of the three phosphotransferase members. (b) A schematic representation of the active-site residues.

group has a low pK_a. In the ATPase, the residue two positions downstream from the Asp351 nucleophile is Thr353. This residue may form a hydrogen bond with the β-phosphate of the ADP leaving group, and serve in the ensuing aspartyl phosphate hydrolysis step by forming a hydrogen bond with the water nucleophile, thus positioning it for attack. The absence of true base catalysis in the hydrolysis step is reminiscent of the use of Asn in the autodephosphorylation of the aspartyl phosphate group of the phosphosensor proteins CheY and NarL (*30*, *31*). As with these signaling proteins, the phosphorylation of the Ca^{2+}-ATPase is for the purpose of switching the protein to an active conformation that then returns to the inactive state upon aspartyl phosphate hydrolysis (*32*, *33*). Mutation of Thr353 in Ca^{2+}-ATPase affects the lifetime of the phosphoenzyme intermediate; its replacement to a hydrophobic residue increases it, while its mutation to an Asp, which can act as a general base, decreases it (*34*).

The β-PGM requires that the sugar oxyanion displaced from the sugar phosphate by the Asp nucleophile is protonated. On the basis of the positioning of the putative active-site Asp8 nucleophile in the phosphoserine phosphatase and ATPase, we might predict that Asp10, which is located two residues downstream from the Asp8 nucleophile, serves in the role of acid/base catalysis. However, the side chain of Asp10 is directed away from the reaction center. This would also account for why the phosphorylated Asp8 is not readily hydrolyzed and, thus, why the phosphorylated form of the enzyme can persist under physiological conditions. The Asp10 carboxylate is not positioned to deprotonate water for in-line attack at the phosphorylated Asp8. The role of acid/base catalyst during β-PGM turnover may be filled by an active-site residue or alternatively, (since the active site is fully accessible to water as assessed by calculating the Connolly's surface with the program VOIDOO (*35*), see Figure 6a), it is conceivable that a water molecule acting alone, or in conjunction with an active site residue, may serve in proton shuttling to the displaced oxyanion. Any further analysis must await the determination of the liganded sugar substrate in the active site via NMR or X-ray crystallographic analysis.

Another specialization in the HAD superfamily is the use of the core in the Ca^{2+}-ATPase where the opening and closing of the channel is in concert with the phosphorylation of the P domain via a protein conformational change. Useful comparisons between the structures of the P domain of the unphosphorylated crystal structure of Ca^{2+}-ATPase (*29*) and phosphorylated β-PGM can be made to analyze the residues involved in the phosphorylation sensing mechanism (see Figure 5). Neither the Mg^{2+} binding residues nor the Lys interactions differ between the phosphorylated and unphosphorylated structures in the HAD superfamily. This leaves Ser/Thr (Ser 114 in β-PGM) as a possible phosphate sensor. In the stably phosphorylated β-PGM, Ser114 forms a hydrogen bond with the phosphate group. On the contrary, in the unphosphorylated structures of the Ca^{2+}ATPse and phosphoserine phosphatase, the corresponding Thr625 and S99, respectively, are not within hydrogen bonding distance (*11*, *36*).

Role of Aspartyl Phosphate as an Intermediate or Signal. In addition to the phosphotransferases of the HAD family, certain 5′-nucleotidases (*37*, *38*), phospholipases, and endonucleases (*39*, *40*) catalyze phosphoryl transfer via aspartyl phosphate intermediates. Also, as alluded to earlier, the aspartyl phosphate group is used by numerous response regulator proteins in signal-transduction pathways (*41*).

The Standard Free Energy for hydrolysis of acetyl phosphate is −10.7 kcal/mol. (*42*). As first noted by Stock et al. (*43*), the high intrinsic energy of the acyl phosphate linkage may be offset by an enzyme according to its function. The substrates of HAD family phosphotransferases alone cover a wide range of energy potentials. High energy potentials exist for the ATP and phosphonoacetaldehyde substrates of the Ca^{2+}-ATPase and phosphonatase. The Standard Free Energy for hydrolysis of the βP−O−Pγ linkage in ATP is −7.6 kcal/mol (*42*). An estimate of the value for the Standard Free Energy for hydrolysis of phosphonoacetaldehyde can be calculated from the equilibrium constant of the phosphonopyruvate to phosphoenol pyruvate (PEP) reaction catalyzed by PEP mutase and the Standard Free Energy for hydrolysis of PEP is −16.6 kcal/mol (*44*). Thus, for both of these phosphotransferases the intrinsic energies of the substrate and aspartyl phosphate intermediate are reasonably matched. This, however, is not

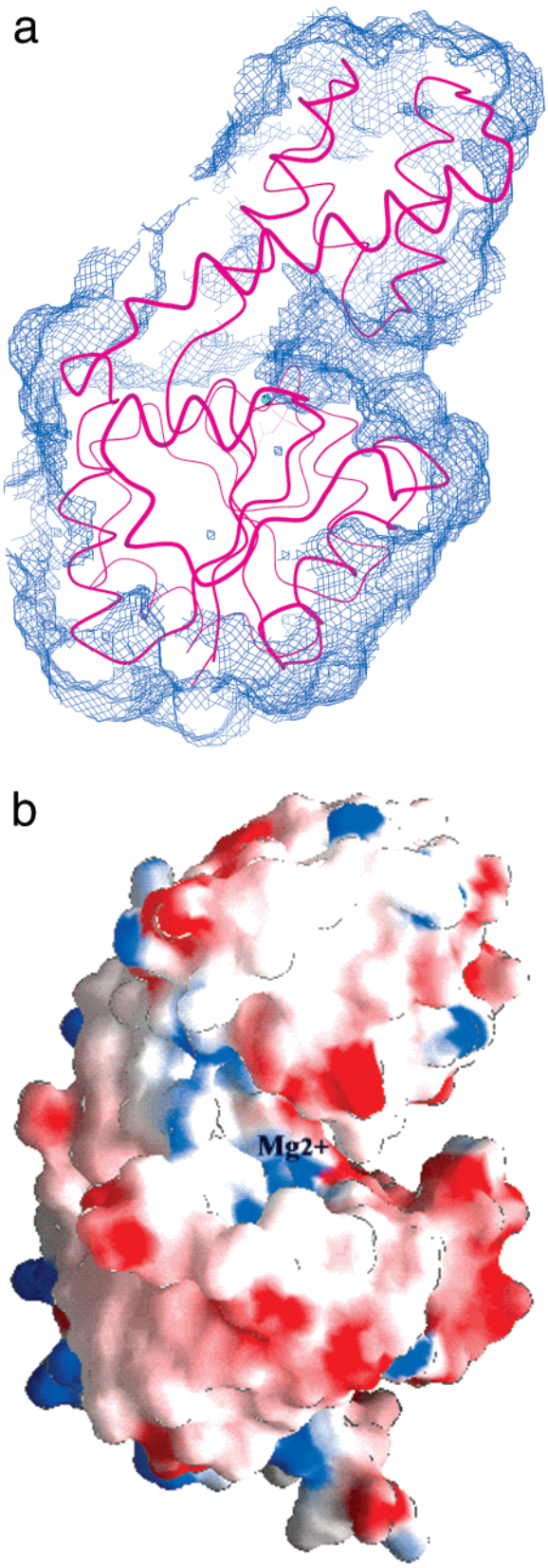

FIGURE 6: Surface representations of phosphorylated β-PGM. (a) Accessiblity to solvent depicted as the Connolly surface (blue cages) calculated with the program VOIDOO using a sphere of 1.3 Å overlayed on the Cα trace of the protein. Phosphoaspartate is shown as a ball-and-stick model to mark the active site. (b) The protein electrostatic surface potential calculated using the program GRASP contoured at −15 kT (red, most negative) and +15 kT (blue, most positive). The active site Mg^{2+} is labeled.

the case for the phosphotransferases acting on simple phosphate monoesters. For example, the P−O linkages in the substrates of β-PGM, G1P (Standard Free Energy for hydrolysis is −5.2 kcal/mol) and G6P (Standard Free Energy for hydrolysis is −3.5 kcal/mol) are significantly lower in energy than is the P−O linkage found in acetyl phosphate. Thus, in the absence of stabilizing interactions by the β-PGM, the reaction of G1P to form the aspartyl phosphate will be 5.5 kcal/mol uphill in energy, and the reaction of G6P will be 7.2 kcal/mol uphill in energy. The interactions between active-site groups may serve to offset the intrinsic energy of the acetyl phosphate group, thereby increasing its thermodynamic stability. The β-PGM structure shows that this is not accomplished simply by a preponderance of positive charge in the active site as demonstrated by the calculation of the electrostatic surface potential using the program GRASP (*45*), see Figure 6b.

The final issue to be addressed is the kinetic stability of the aspartyl phosphate group. As was noted above, many of the HAD family phosphotransferases form the acyl phosphate as a chemical intermediate en route to hydrolysis of the phosphate ester substrate, while the Ca^{2+}-ATPase forms the acyl phosphate as a mechanism to induce a conformational change in the enzyme necessary for ion transport across biomembranes. The fast rate of aspartyl phosphate hydrolysis observed for the phosphatases is ensured by base catalysis, which for the phosphoserine phosphatase derives from the proximal Asp13. A slower rate of hydrolysis is needed for the Ca^{2+}-ATPase aspartyl phosphate group to allow time for the chemically coupled conformational change to occur before hydrolysis. The attenuated hydrolysis rate is accomplished by use of Thr (Thr353) in place of the Asp (Figure 5a,b). The Thr can serve as a water-binding residue but cannot contribute to the rate of the hydrolysis reaction as a general base. In β-PGM, the corresponding Asp residue (Asp10) is oriented away from aspartyl phosphate. At this position, it cannot bind and activate a water molecule for in-line attack at the aspartyl phosphate group. Thus, in the HAD family of phosphotransferases the lifetime of the aspartyl phosphate appears to be determined by the presence of a water-binding residue and by whether this residue can serve as a general base.

An analogous conclusion was drawn earlier with regard to the lifetime of the aspartyl phosphate group found in the response regulator proteins. Zapf et al. (*46*) examined the lifetime of the aspartyl phosphate group of the response regulator protein Spo0F and, based on mutagenesis data and comparison of group usage among the response regulator protein family members, concluded that autophosphatase activity among the aspartyl phosphate response regulator proteins is determined in part by the nature of the side chain positioned to bind and activate the water nucleophile.

The need for a water activating group to assist in the autodephosphorylation of a protein aspartyl phosphate group, whether it be located on the protein surface such as in the response regulator family, or buried in the active site such as in the HAD family phosphatases, suggests that despite its high energy the aspartyl phosphate group is kinetically stable under physiological conditions. In examining the literature on acetyl phosphate hydrolysis, we found that the aspartyl phosphate group might be expected to persist under physiological conditions for several hours. Di Sabato and

Jencks (*47*) reported that the rate of hydrolysis of acetyl phosphate is pH independent between pH 2.5 and 7.5 and that at pH 6.9, 39 °C, the $t_{1/2}$ is 2.7 h, and at 25 °C the $t_{1/2}$ is 21 h.

Thus, the Asp residue may have been selected by nature to function in phosphoryl transfer in part because of its nucleophilicity but also in part because of the moderate kinetic stability of the acyl phosphate group. The lifetime of the aspartyl phosphate group might be increased through water exclusion from surrounding areas, while its lifetime can be decreased in a very incremental manner through the positioning of a residue nearby, which, depending on its structure, can serve to bind and activate water with a predetermined efficiency.

ACKNOWLEDGMENT

We wish to thank Dr. Marc C. Morais for help with data collection.

NOTE ADDED AFTER ASAP POSTING

This paper was posted to the web on June 5, 2002 before final corrections were made. Glu169 residues were mistakenly referred to as Asp169 in the text. The correct text appears in this version posted June 25, 2002.

REFERENCES

1. Qian, N., Stanley, G. A., Hahn-Hagerdal, B., and Radstrom, P. (1994) Purification and characterization of two phosphoglucomutases from *Lactococcus lactis subsp. lactis* and their regulation in maltose- and glucose-utilizing cells. *J. Bacteriol. 176*, 5304−5311.
2. Qian, N., Stanley, G. A., Bunte, A., and Radstrom, P. (1997) Product formation and phosphoglucomutase activities in *Lactococcus lactis*: cloning and characterization of a novel phosphoglucomutase gene. *Microbiology 143*, 855−865.
3. Dai, J. B., Liu, Y., Ray, W. J. Jr., and Konno, M. (1992) The crystal structure of muscle phosphoglucomutase refined at 2.7-angstrom resolution. *J. Biol. Chem. 267*, 6322−6337.
4. Hisano, T., Hata, Y., Fujii, T., Liu, J. Q., Kurihara, T., Esaki, N., and Soda, K. (1996) Crystal structure of L-2-haloacid dehalogenase from *Pseudomonas sp.* YL. An alpha/beta hydrolase structure that is different from the alpha/beta hydrolase fold. *J. Biol. Chem. 271*, 20322−20330.
5. Koonin, E. V., and Tatusov, R. L. (1994) Computer analysis of bacterial haloacid dehalogenases defines a large superfamily of hydrolases with diverse specificity. Application of an iterative approach to database search. *J. Mol. Biol. 244*, 125−132.
6. Ridder, I. S., and Dijkstra, B. W. (1999) Identification of the Mg^{2+}-binding site in the P-type ATPase and phosphatase members of the HAD (haloacid dehalogenase) superfamily by structural similarity to the response regulator protein CheY. *Biochem. J. 339*, 223−226.
7. Naught L. E., and Tipton P. A. (2001) Kinetic mechanism and pH dependence of the kinetic parameters of *Pseudomonas aeruginosa* phosphomannomutase/phosphoglucomutase. *Arch. Biochem. Biophys. 396*, 111−118.
8. Shankar, S., Ye, R. W., Schlictman, D., and Chakrabarty, A. M. (1995) Exopolysaccharide alginate synthesis in *Pseudomonas aeruginosa*: enzymology and regulation of gene expression. *Adv. Enzymol. RAMB 70*, 221−255.
9. Ray, W. J., Jr., Burgner, J. W., II, and Post, C. B. (1990) Characterization of vanadate-based transition-state-analogue complexes of phosphoglucomutase by spectral and NMR techniques. *Biochemistry 29*, 2770−2778.
10. Morais, M. C, Zhang, W., Baker, A. S., Zhang, G., Dunaway-Mariano, D., and Allen, K. N. (2000) The crystal structure of *Bacillus cereus* phosphonoacetaldehyde hydrolase: insight into catalysis of phosphorus bond cleavage and catalytic diversification within the HAD enzyme superfamily. *Biochemistry 39*, 10385−10396.
11. Wang, W., Kim, R., Jancarik, J., Yokota, H., and Kim, S. H. (2001) Crystal structure of phosphoserine phosphatase from *Methanococcus jannaschii*, a hyperthermophile, at 1.8 Å resolution. *Structure 9*, 65−71.
12. Lahiri, S. D., Zhang, G., Radstrom, P., Dunaway-Mariano, D., and Allen, K. N. (2002) Crystallization and preliminary X-ray diffraction studies of β-phosphoglucomutase from *Lactococcus lactus. Acta Crystallogr. D Biol. Crystallogr. 58*, 324−326.
13. Matthews, B. W. (1985) Determination of protein molecular weight, hydration, and packing from crystal density. *Methods Enzymol. 114*, 176−187.
14. Guss, J. M., Merritt, E. A., Phizackerley, R. P., Hedman, B., Murata, M., Hodgson, K. O., and Freeman, H. C. (1988) Phase determination by multiple-wavelength X-ray diffraction: crystal structure of a basic "blue" copper protein from cucumbers. *Science 241*, 806−811.
15. Hendrickson, W. A., Horton, J. R., and LeMaster, D. M. (1990) Selenomethionyl proteins produced for analysis by multiwavelength anomalous diffraction (MAD): a vehicle for direct determination of three-dimensional structure. *EMBO J. 9*, 1665−1672.
16. Otwinowski, Z., and Minor, W. (1997) Processing of X-ray Diffraction Data Collected in Oscillation Mode. *Methods Enzymol. 276*, 307−326.
17. Terwilliger, T. C., and Berendzen., J. (1999) Automated structure solution for MIR and MAD. *Acta Crystallogr. D55*, 849−861.
18. Terwilleger, T. C. (1999) Reciprocal-space solvent flattening. *Acta Crystallogr. D55*, 1863−1871.
19. Jones, T. A, Zou, J.-Y., Cowan, S. W., and Kjeldgaard, M. (1991) Improved methods for building protein models in electron density maps and the location of errors in these models. *Acta Crystallogr. A47*, 110−119.
20. Read, R. J. (1997) Model phases: probabilities and bias. *Methods Enzymol. 278*, 110−128.
21. Brunger A. T., Kuriyan J., and Karplus M. (1987) Crystallographic R factor Refinement by Molecular Dynamics. *Science 235*, 458−460.
22. Pontius, J., Richelle, J., and Wodak, S. J. (1996) Deviations from standard atomic volumes as a quality measure for protein crystal structures. *J. Mol. Biol. 264*, 121−36.
23. Altschul, S. F., Gish, W., Miller, W., Myers, E. W., and Lipman, D. J. (1990) Basic local alignment search tool. *J. Mol. Biol. 215*, 403−410.
24. Collet, J. F., Stroobant, V., Pirard, M., Delpierre, G., and Van Schaftingen, E. (1998) A new class of phosphotransferases phosphorylated on an aspartate residue in an amino-terminal DXDX(T/V) motif. *J. Biol. Chem. 273*, 14107−14112.
25. Ridder, I. S., Rozeboom, H. J., Kalk, K. H., Janssen, D. B., and Dijkstra, B. W. (1997) Three-dimensional structure of L-2-haloacid dehalogenase from *Xanthobacter autotrophicus* GJ10 complexed with the substrate-analogue formate. *J. Biol. Chem. 272*, 33015−33022.
26. Baker, A. S., Ciocci, M. J., Metcalf, W. W., Kim, J., Babbitt, P. C. Wanner, B. L., Martin, B. M., and Dunaway-Mariano, D. (1998) Insights into the mechanism of catalysis by the P−C bond-cleaving enzyme phosphonoacetaldehyde hydrolase derived from gene sequence analysis and mutagenesis. *Biochemistry 37*, 9305−9331.
27. Aravind, L., Galperin, M. Y., and Koonin, E. V. (1998) The catalytic domain of the P-type ATPase has the haloacid dehalogenase fold. *Trends Biochem. Sci. 23*, 127−129.
28. Stokes, D. L., and Green, N. M. (2000) Modeling a dehalogenase fold into the 8-Å density map for Ca(2+)-ATPase defines a new domain structure. *Biophys. J. 78*, 1765−1776.
29. Toyoshima, C., Nakasako, M., Nomura, H., and Ogawa, H. (2000) Crystal structure of the calcium pump of sarcoplasmic reticulum at 2.6 Å resolution. *Nature 405*, 647−655.
30. Baikalov, I., Schroder, I., Kaczor-Grzeskowiak, M., Grzeskowiak, K., Gunsalus, R. P., and Dickerson, R. E. (1996) Structure of the *Escherichia coli* response regulator NarL. *Biochemistry 35*, 11053−11061.
31. Lee, S. Y., Cho, H. S., Pelton, J.G., Yan, D., Berry, E. A., and Wemmer, D. E. (2001) Crystal structure of activated CheY. Comparison with other activated receiver domains. *J. Biol. Chem. 276*, 16425−16431.
32. MacLennan, D. H., and Green, N. M. (2000) Structural biology. Pumping ions. *Nature 405*, 633−634.
33. McIntosh, D. B. (2000) Portrait of a P-type pump. *Nat. Struct. Biol. 7*, 532−535.

34. Clausen, J. D., McIntosh, D. B., Woolley, D. G., and Andersen, J. P. (2001) Importance of Thr-353 of the conserved phosphorylation loop of the sarcoplasmic reticulum Ca^{2+}-ATPase in MgATP binding and catalytic activity. *J. Biol. Chem. 276*, 35741−35750.
35. Kleywegt, G. J., and Jones, T. A. (1994) Detection, delineation, measurement and display of cavities in macromolecular structures. *Acta Crystallogr. D 50*, 178−185.
36. Cho, H., Wang, W., Kim, R., Yokota, H., Damo, S., Kim, S. H., Wemmer, D., Kustu, S., and Yan, D. (2001) BeF_3^- acts as a phosphate analogue in proteins phosphorylated on aspartate: structure of a BeF_3^- complex with phosphoserine phosphatase. *Proc. Natl. Acad. Sci. U.S.A. 98*, 8525−8530.
37. Allegrini, S., Ferrara, L., Pesi, R., Pinna, P., Sgarrella, F., Camici, M., Ericksson, S., and Tozzi, M. G. (2001) Bovine cytosolic 5′-nucleotidase acts through the formation of an aspartate 52-phosphoenzyme intermediate. *J. Biol. Chem. 276*, 33526−33532.
38. Stelte, B., and Witzel, H. (1986) Formation of an aspartyl phosphate intermediate in the reactions of nucleoside phosphotransferase from carrots. *Eur. J. Biochem. 155*, 121−124.
39. Ponting, C. P., and Kerr, I. D. (1996) A novel family of phospholipase D homologues that includes phospholipid synthases and putative endonucleases: identification of duplicated repeats and potential active site residues. *Protein Sci. 5*, 914−922.
40. Koonin, E. V. (1996) A duplicated catalytic motif in a new superfamily of phosphohydrolases and phospholipid synthases that includes poxvirus envelope proteins. *Trends Biol. Sci. 21*, 242−243.
41. Lee, S. Y., Ho, S. C., Pelton, J. G., Yan, D., Berry, E. A., and Wemmer, D. E. (2001) Crystal structure of activated CheY. Comparison with other activated receiver domains. *J. Biol. Chem. 276*, 16425−16431.
42. Jencks, W. P. (1976) in *Handbook of Biochemistry and Molecular Biology* (Fasman, G. D., Ed.) 3rd ed., Physical and Chemical Data, Vol I, pp 296−304, CRC Press, Boca Raton, FL.
43. Stock, J. B., Stock, A. M., and Mottonen, J. M. (1990) Signal transduction in bacteria. *Nature 344*, 395−400.
44. Kim, J., and Dunaway-Mariano, D. (1996) Phosphoenolpyruvate mutase catalysis of phosphoryl transfer in phosphoenolpyruvate: kinetics and mechanism of phosphorus−carbon bond formation. *Biochemistry 35*, 4628−4635.
45. Nicholls, A., Sharp, K. A., and Honig, B. (1991) Protein folding and association: insights from the interfacial and thermodynamic properties of hydrocarbons. *Proteins: Struct., Funct. and Genet. 11*, 281−296.
46. Zapf, J., Madhusudan, M., Grimshaw, C. E., Hoch, J. A., Varughese, K. I., and Whitetely, J. M. (1998) A source of response regulator autophosphatase activity: the critical role of a residue adjacent to the Spo0F autophosphorylation active site. *Biochemistry 37*, 7725−7732.
47. Di Sabato, G., and Jencks, W. P. (1961) Mechanism and Catalysis of Reactions of Acyl Phosphates. II. Hydrolysis *J. Am. Chem. Soc. 83*, 4400−4405.

BI0202373